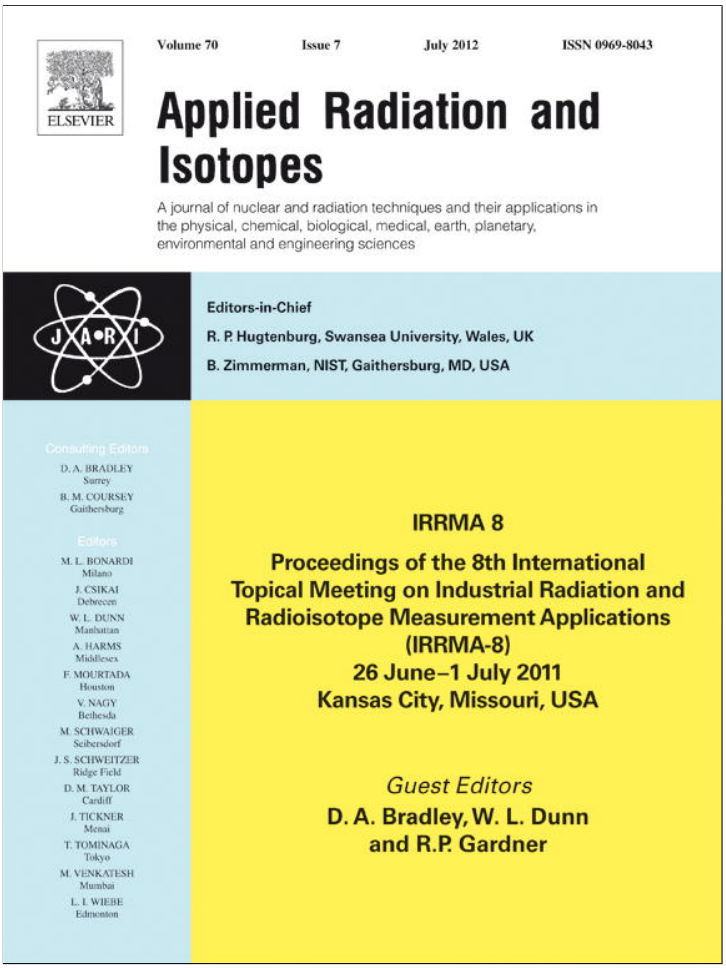

Applied Radiation and Isotopes 70 (2012) 1186–1192

Contents lists available at ScienceDirect

Applied Radiation and Isotopes

journal homepage: www.elsevier.com/locate/apradiso

Quantitative comparison between experimental and simulated gamma-ray spectra induced by 14 MeV tagged neutrons

B. Perot [a,*], W. El Kanawati [a], C. Carasco [a], C. Eleon [a], V. Valkovic [b], D. Sudac [c], J. Obhodas [c], G. Sannie [d]

[a] CEA, DEN, Cadarache, Nuclear Measurement Laboratory, F-13108 Saint-Paul-lez-Durance, France
[b] A.C.T.d.o.o., Prilesje 4, 10000 Zagreb, Croatia
[c] Ruder Boskovic Institute, Bijenicka c. 54, 10000 Zagreb, Croatia
[d] CEA, LIST, Saclay, F-91191 Gif-sur-Yvette, France

ARTICLE INFO

Available online 18 July 2011

Keywords:
Fast neutron analysis
Associated particle technique
Explosive detection
Monte Carlo simulation

ABSTRACT

Fast neutron interrogation with the associated particle technique can be used to identify explosives in cargo containers (EURITRACK FP6 project) and unexploded ordnance on the seabed (UNCOSS FP7 project), by detecting gamma radiations induced by 14 MeV neutrons produced in the $^{2}H(^{3}H,\alpha)n$ reaction. The origin of the gamma rays can be determined in 3D by the detection of the alpha particle, which provides the direction of the opposite neutron and its time-of-flight. Gamma spectroscopy provides the relative counts of carbon, nitrogen, and oxygen, which are converted to chemical fractions to differentiate explosives from other organic substances. To this aim, Monte Carlo calculations are used to take into account neutron moderation and gamma attenuation in cargo materials or seawater. This paper presents an experimental verification that C, N, and O counts are correctly reproduced by numerical simulation. A quantitative comparison is also reported for silicon, iron, lead, and aluminium.

1. Introduction

Fast neutron interrogation can be used in a variety of areas (Buffler and Tickner, 2010) to identify materials, especially for explosive detection. The associated particle technique (Valkovic et al., 1969) has been applied in EU projects like EURITRACK, Eritr@C, and UNCOSS, in which extensive databases of gamma-ray signatures induced by 14 MeV neutrons on individual elements (C, N, O, Na, Al, Si, Cl, K, Ca, Cr, Fe, Ni, Cu, Zn, Pb, etc.) have been produced and compared to MCNP simulations (Perot et al., 2008; El Kanawati et al., 2011a,b). Attention has been focused on main peaks and neutron scattering continuum, showing a satisfactory qualitative agreement for C, N, and O spectra used for explosive identification. The gamma-ray spectrum of an unknown interrogated material is fitted with a linear combination of these elemental signatures to determine their relative count fractions, which are then converted to chemical proportions taking into account gamma-ray production cross sections for the neutron energy spectrum reaching the target materials, and photon attenuation between the target and gamma-ray detectors (Carasco et al., 2007). This reference reports an approach mixing Monte Carlo simulation of neutron transport and gamma energy deposition in the detector with analytical calculation of photon attenuation. A new approach entirely based on Monte Carlo simulation is now possible, thanks to recent developments in MCNP output file processing (Carasco, 2010), allowing realistic time–energy resolution and counting statistics descriptions. New sets of correction factors are being produced within Eritr@C (because EURITRACK's low-energy threshold was reduced from 1.35 to 0.6 MeV to improve the detection of some elements; El Kanawati et al., 2010) and UNCOSS projects. MCNPX RSICC has been used, instead of MCNP 4C in (Carasco et al., 2007), and the ENDF/B-VII.0 data library instead of ENDF/B-VI.0. Results will be reported soon, the aim of this paper being to verify that numerical simulation quantitatively reproduces the counts in gamma-ray spectra of well-known samples of graphite (for carbon), water (for oxygen), and melamine ($C_3H_6N_6$ for nitrogen and carbon). Comparisons for other materials frequently found in cargo containers (Obhodas et al., 2010) or part of the EURITRACK portal are also presented: wood (C_{22} $H_{31}O_{12}$), silicon dioxide sand, aluminium, iron, and lead blocks.

The gamma-ray production cross sections reported in Simakov et al. (1998) indeed show large discrepancies between experimental data, and inconsistencies in the evaluated data libraries like ENDF/B-V and ENDF/B-VI have also been observed (Bendahan et al., 1995), even for well-known elements like C, N, and O. The ENDF/B-VI.0 database used in Carasco et al. (2007) also did not reproduce the anisotropic gamma-ray production, contrary to ENDF/B-VII.0, which is of importance when inspecting different areas inside a cargo container with a large variety of beam-to-detector angles.

* Corresponding author. Tel.: +33 442254048; fax: +33 442252367.
E-mail address: bertrand.perot@cea.fr (B. Perot).

0969-8043/$ - see front matter © 2011 Elsevier Ltd. All rights reserved.
doi:10.1016/j.apradiso.2011.07.005

2. Experiment vs. MCNP simulation

The samples described in Table 1 have been measured with the geometry shown in Fig. 1.

The pyramidal tagged neutron beam has been modelled with the conical source of MCNP, which has been shaped to the square experimental beam with a frame selecting only the neutrons in the appropriate solid angle. The neutron-induced photon flux is estimated using "point detectors" (MCNP type 5 tally) located above the target, between the two parallel rows of EURITRACK top detectors. The photon flux is then used as a source in a second calculation of their energy deposition in the NaI(Tl) $5'' \times 5'' \times 10''$ detectors, using the MCNP "pulse height tally" (F8). In this second calculation, the photons are injected under a normal incidence in the small face ($5'' \times 5''$) of the detectors. MODAR software is used to fasten this two-step calculation by implementing pre-calculated response functions of the detector based on F8 calculations taking into account the energy resolution observed experimentally (Carasco, 2010). To limit the bias due to incidence angle, only the three pairs of top detectors located above the target have been used.

The neutron time-of-flight (TOF) spectrum of the graphite sample acquisition is shown in Fig. 2 (top panels). The random background observed in the negative times has been subtracted from the other areas of interest. The first peak near 10 ns is due to tagged neutron interactions in the walls of the generator and surrounding materials. The main peak due to graphite centred at about 31 ns overlaps with a smaller signal due to tagged neutrons scattered by the sample towards the NaI(Tl) detectors, surrounding iron structures and lead collimators. Selecting the graphite TOF window provides the expected gamma spectrum of carbon (middle, left panel), with its full-energy and escape peaks, whereas the scattered neutron spectrum (middle, right panel) does not reveal noticeable gamma signature. The fraction of scattered neutron signal overlapping in the graphite TOF window has been estimated to be 16% using Gaussian functions (top, right panel), and it has been subtracted to obtain the net carbon spectrum (bottom panel).

The agreement between experiment and MCNP is satisfactory, taking into account the following sources of uncertainty, which will also apply for all further samples.

1. Fig. 2 shows significant statistical fluctuations due to limited acquisition time in Rijeka seaport, where the EURITRACK system is under operation (Carasco et al., 2008), and to the use of only six detectors above the target to limit the gamma angle of incidence.
2. Systematic uncertainties must also be taken into account, of which the most important is certainly the precision of the nuclear data used in MCNP. Relative standard deviations of the experimental data reported in Simakov et al. (1998) are generally 10–20%, but they are much larger for a number of gamma rays. As already mentioned the construction of evaluated nuclear data files also suffers from proper uncertainties (Carasco et al., 2008).
3. Modelling and calculation methods introduce uncertainties in the geometry and material descriptions. The injection of the photon flux perpendicular to the detector entrance surface to calculate energy deposition is an example of modelling approximation.
4. Count losses in the data acquisition system can be a source of uncertainty but the alpha–gamma coincidence rate was only about 3000 s^{-1}. The EURITRACK front-end electronics dead-time being close to 5 μs, essentially due to the QDC conversion time (Lunardon et al., 2007), count losses are lower than 1.5%.
5. A filtering algorithm is used to suppress multiple alpha or gamma hits, and other unwanted events. The filtering ratio of good to total events is significant, typically 50%, and only good events have been used to scale calculation for a quantitative comparison with experiment. However a fraction of the rejected

Table 1
Characteristics of the modelled experiments.

Target	Source to target distance (cm)	Target to detector distance (cm)	Density	Dimensions		
				X (cm)	Y (cm)	Z (cm)
Graphite	104	89	1.75	20	30.1	20
Water	103	96	1	25	14	14
Lead	95	100	11.2	5	20	40
Iron	96	97	7.4	1	41	44.5
Melamine	95	89	0.95	15	20	10
Wood	101	91	0.6	46	40	17
Silicon dioxide	85	93	1.75	15	20	6
Aluminium	94.5	100	2.66	Diameter = 20 cm		22.5

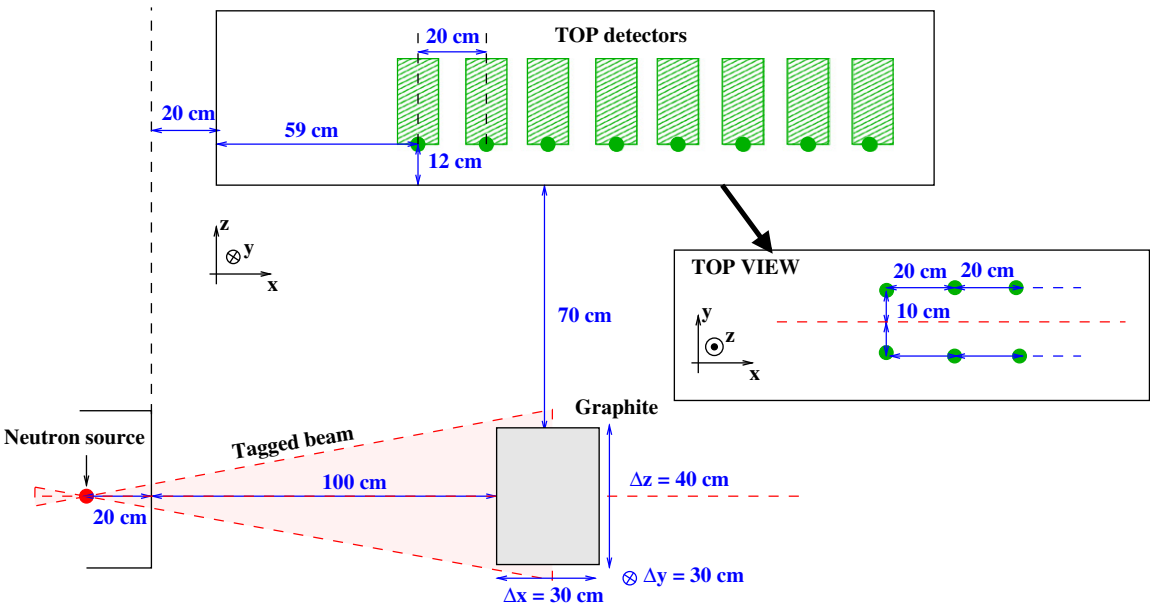

Fig. 1. Setup of the graphite target acquisition. The points below the $5'' \times 5'' \times 10''$ NaI(Tl) top detectors represent the location of the MCNP point detectors.

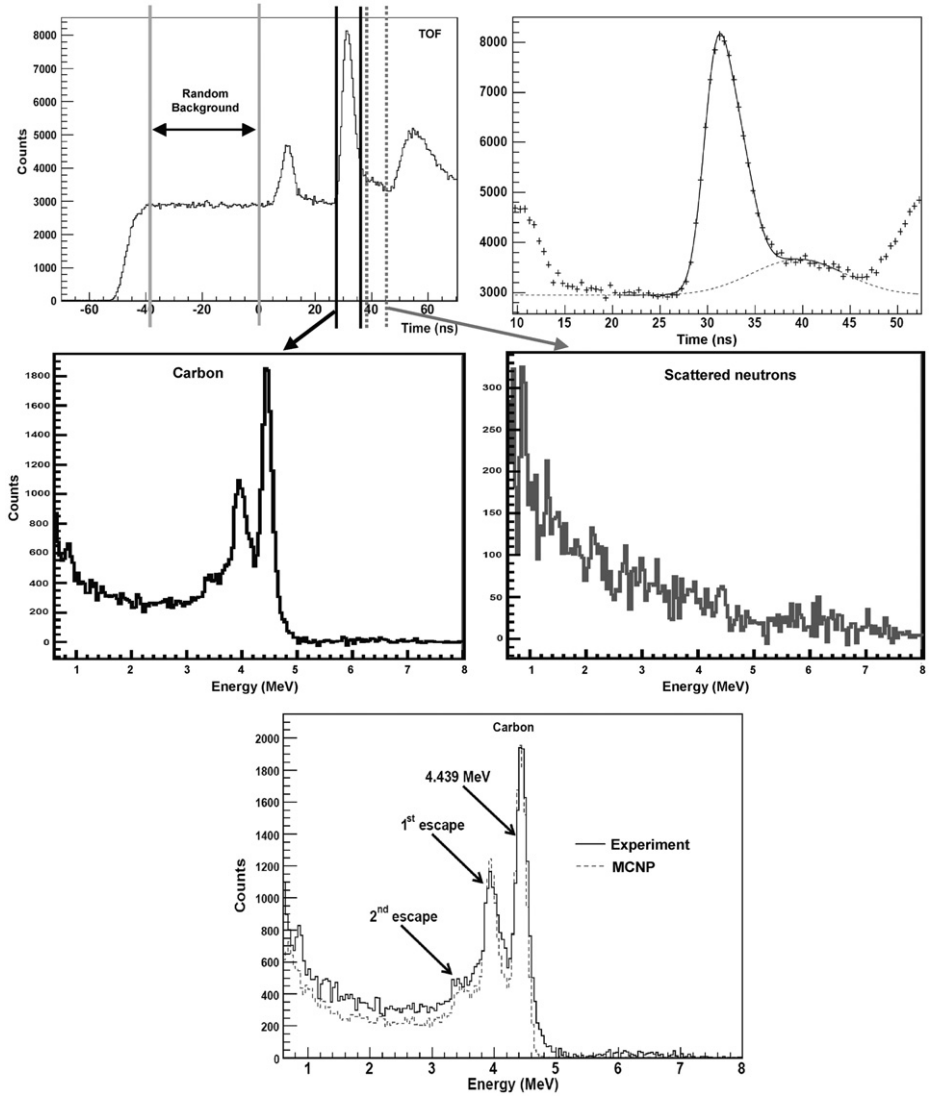

Fig. 2. Graphite acquisition TOF spectrum (above, left) fitted with Gaussian functions (on the right): full line for graphite peak at 30–35 ns and dotted line for scattered neutrons. In the middle, gamma-ray spectra corresponding to the graphite (on the left) and scattered neutron (on the right) TOF windows. Below, the net experimental gamma spectrum of carbon after subtraction of the scattered neutron contribution (full line), and the simulated spectrum (dotted line).

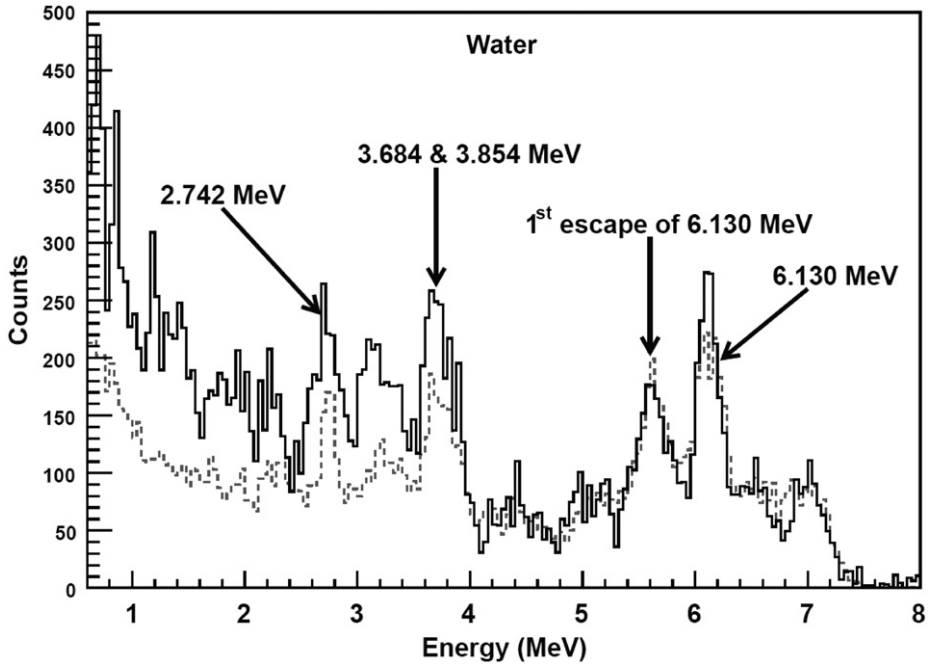

Fig. 3. Gamma-ray spectrum of the water target after subtraction of the scattered neutron contribution (full line), and simulated spectrum of oxygen (dotted line).

events could appear in the simulated spectra, such as gamma rays produced in a cascade electromagnetic relaxation of a nucleus excited by a single tagged neutron. The fraction of events rejected due to a gamma multiplicity larger than one is here smaller than 10%, among which for cascade gamma rays the bias does not exceed a few percents.

To summarise we have estimated that the average relative standard deviation associated with the simulated spectrum is about 20%, which is certainly underestimated for gamma rays with obvious nuclear data errors (as will be shown below for the 3.089 MeV line of oxygen) and overestimated for well-known data like the carbon 4.439 MeV line.

A water target has been used to assess the oxygen spectrum shown in Fig. 3. As previously for graphite, the scattered neutron signal has been estimated with Gaussian fits (here about 28% of the signal in the water window TOF) and subtracted to obtain the net oxygen spectrum. Fast neutrons do not produce gamma radiation on hydrogen nuclei. The agreement between simulation and experiment is quite correct taking into account statistical fluctuations and the systematic uncertainties mentioned above, but the 3.089 MeV gamma-ray due to the relaxation of the first excited level of ^{13}C, following the $^{16}O(n,\alpha)^{13}C$ reaction, is largely underestimated by the simulation as already observed qualitatively in Perot et al. (2008), El Kanawati et al. (2011a,b), and Evsenin et al. (2009).

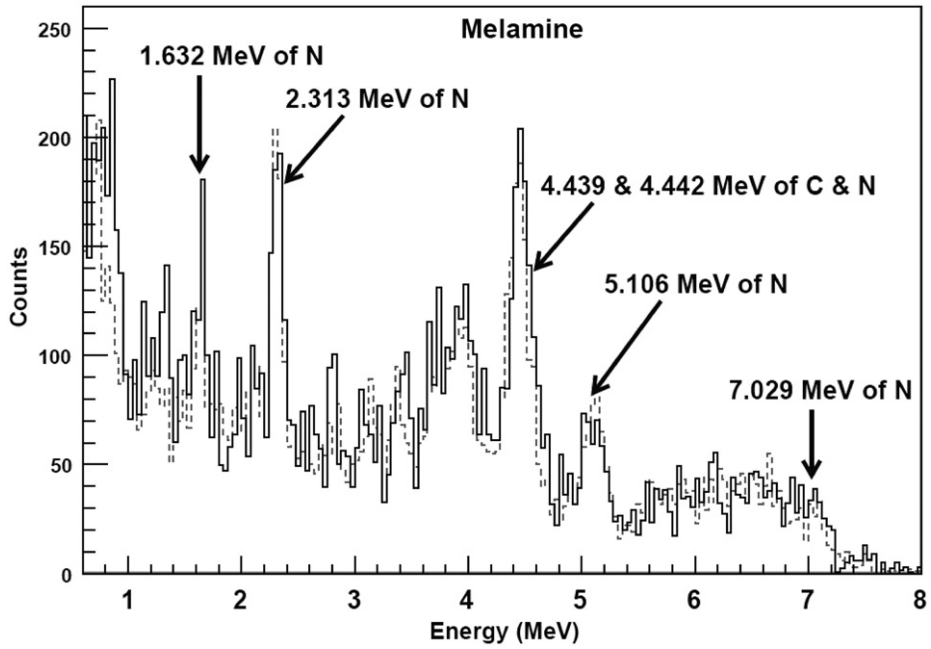

Fig. 4. Measured (full line) and simulated (dotted line) gamma-ray spectra of melamine.

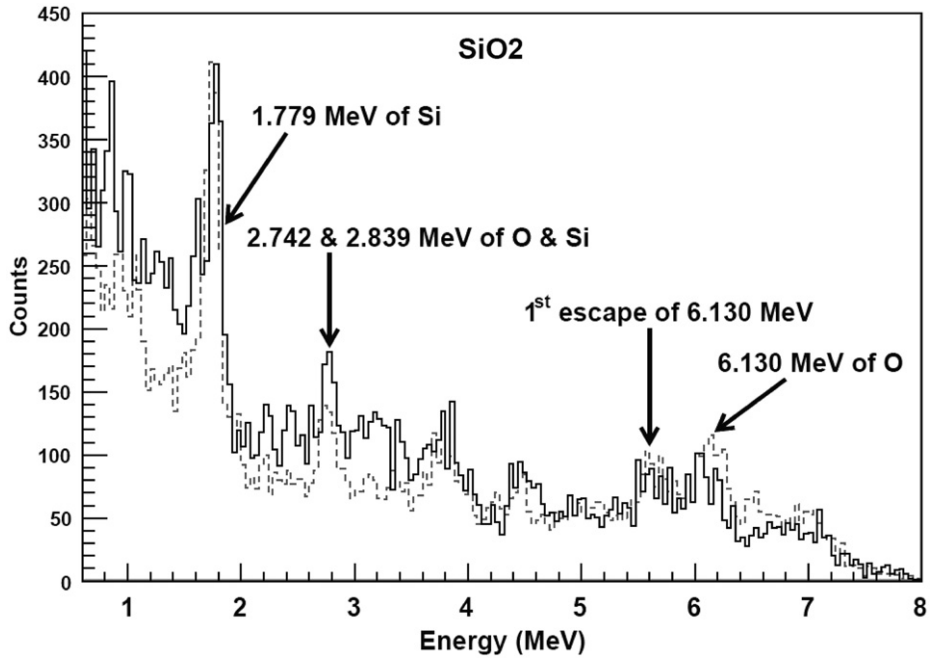

Fig. 5. Measured (full line) and simulated (dotted line) gamma-ray spectra of sand.

A melamine sample ($C_3H_6N_6$) has been used to check nitrogen gamma rays. The net spectrum after subtraction of about 2% of scattered neutrons is shown in Fig. 4. The agreement between simulation and experiment is satisfactory within statistical and systematic uncertainties.

SiO_2 sand has been used to validate the simulation of silicon. This element is often observed in cargo containers transporting ceramics, glass, fibreglass wool, etc. and in sediments in the case of explosive detection on the seafloor. Fig. 5 shows the net SiO_2 spectrum after subtracting about 10% of scattered neutron events. Simulation correctly reproduces the measured spectrum.

Wood ($H_{31}C_{22}O_{12}$) is also frequently found in cargo containers in the form of raw material or manufactured goods (furniture, toys, etc). Fig. 6 shows the wood spectrum, for which simulation and experiment agree satisfactorily except for the 3.089 MeV gamma ray of oxygen. No scattered neutron subtraction was performed here, their fraction being here estimated to be only 1.6%.

A few metallic elements have also been investigated. Iron is frequently observed in cargo containers (Simakov et al., 1998) transporting machines, tools, car pieces, pipes, nails, wire mesh grids, etc. In the EURITRACK system, lead is used to shield the detectors and can be observed when the volume of interest is close to the top of the container because part of the tagged neutrons are scattered towards the detectors and shields. Aluminium can also be found in the containers. Figs. 7–9 show a significant underestimation of the counts by numerical simulation, even if the main

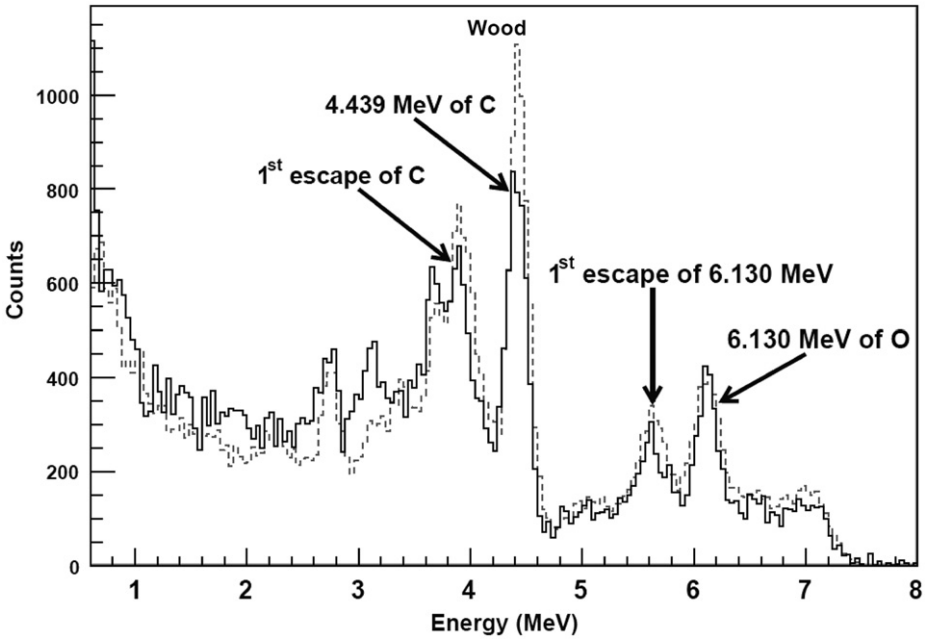

Fig. 6. Measured (full line) and simulated (dotted line) gamma-ray spectra of wood.

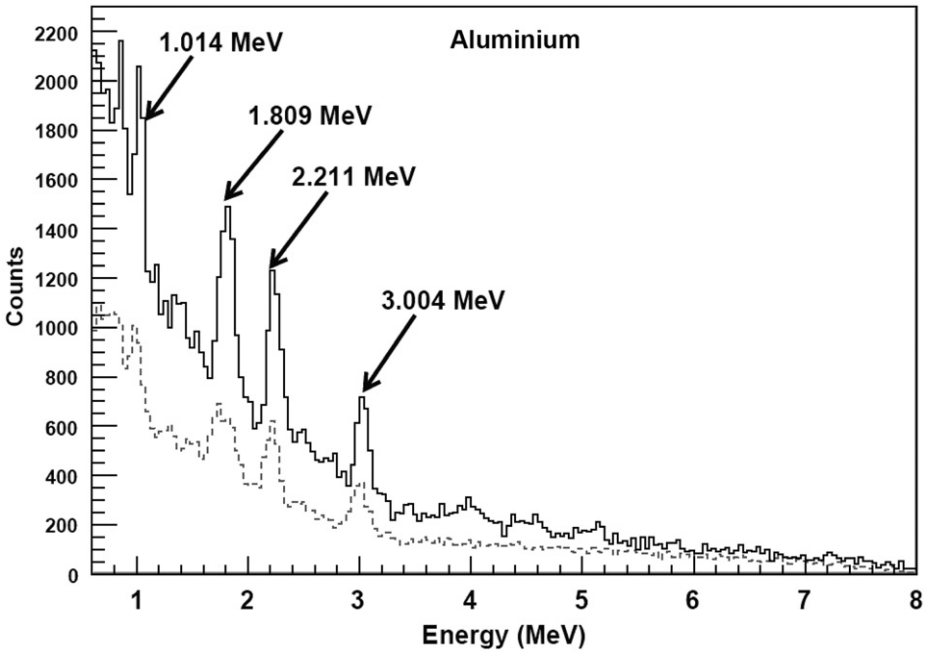

Fig. 7. Measured (full line) and simulated (dotted line) gamma-ray spectra of aluminium.

expected peaks are present. No subtraction of the scattered neutron contribution has been necessary in the experimental spectra. It must be noted that the anisotropy of the gamma-ray production is not described in the ENDFB/VII.0 database for Al, Fe, and Pb, which can be another cause of the observed discrepancy in addition to the uncertainty on the average cross sections already mentioned above and reported in Simakov et al. (1998). For instance, the angular distribution of the 0.847 MeV gamma ray of ^{56}Fe shows a minimum at 90° (Day and Walt, 1960), which is the average angle in our measurements; see Fig. 1 (only the three pairs of detectors located above the target are used). On the other hand, gamma attenuation is very large in these dense samples, but a sensitivity study has been performed by varying the density in a [−10%, +10%] range without showing a significant modification of the calculated spectra. Finally, an unidentified bias in all the simulated spectra (graphite, water, wood, melamine, silicon dioxide sand, iron, lead, and aluminium) cannot be excluded to explain the underestimation observed in the case of Fe, Pb, and Al. If present, such a bias would mean that simulation is overestimating the other spectra. In any case the important outcome of this work, in view of further calculations, is that the C, N, and O signatures are reproduced with the same relative intensity by numerical simulation.

3. Conclusion

The gamma-ray spectra produced by 14 MeV tagged neutron beams of the EURITRACK system in thick samples of graphite,

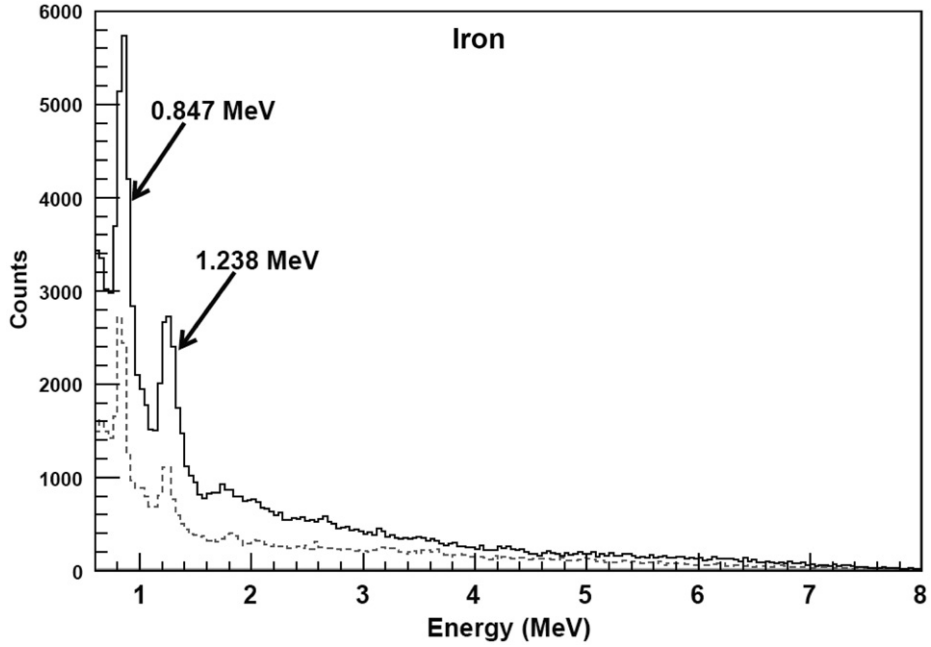

Fig. 8. Measured (full line) and simulated (dotted line) gamma-ray spectra of iron.

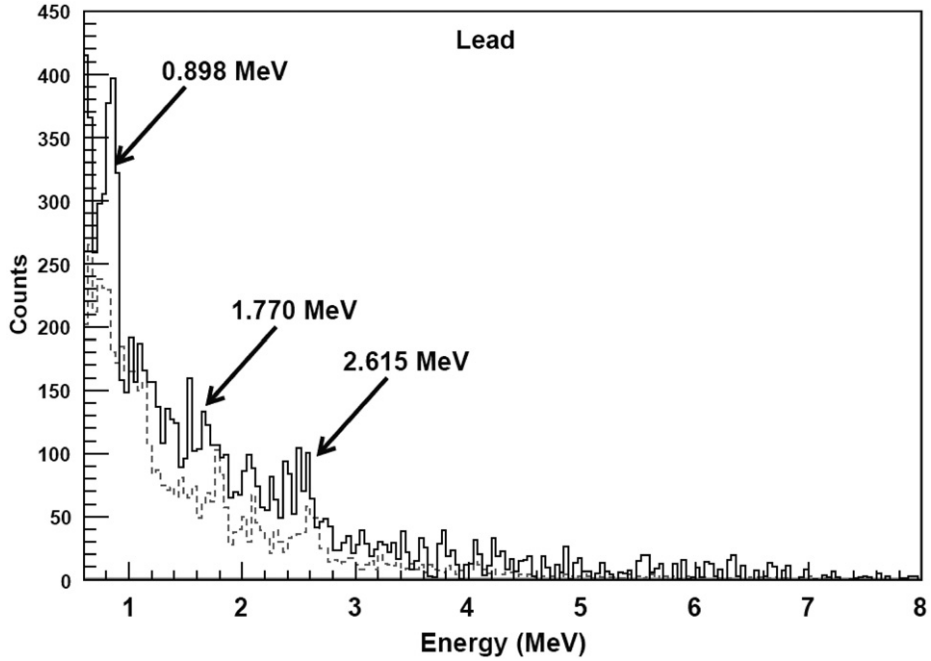

Fig. 9. Measured (full line) and simulated (dotted line) gamma-ray spectra of lead.

water, melamine, wood, and silicon dioxide sand are correctly reproduced by MCNPX calculations with the ENDF/B-VII.0 library. This result shows that Monte Carlo simulation can be used to convert the C, N, and O count ratios into chemical proportions. The calculation of these conversion factors, taking into account neutron slowing down and photon attenuation in cargo containers, and their experimental qualification will be detailed in another paper (El Kanawati et al., 2011a,b). For instance the obtained O/C chemical ratio for the wood target is 0.59 ± 0.04, which is in good agreement with the 0.545 proportion in wood ($C_{22}H_{31}O_{12}$), and nitrogen is not detected by the unfolding algorithm. For the melamine target ($C_3H_6N_6$) the measured N/C ratio is 2.16 ± 0.62, which is also consistent with the real one, and a small oxygen fraction is detected but it is not significant regarding statistical uncertainty.

On the other hand, the characteristic peaks and continuum of the iron, aluminium, and lead spectra are qualitatively reproduced by MCNPX calculations, but the counts in the spectra are underestimated with respect to experiment. Therefore a conversion of the unfolded counts into chemical fractions based on numerical simulation would certainly be biased but it is not used in the EURITRACK and UNCOSS applications, which only rely on the C, N, and O proportions to differentiate explosives, illicit drugs, and benign organic materials.

Acknowledgments

This work is supported by the European Union through the Eritr@C project, referenced as JLS/2007/ISEC/550. EU has also supported the FP6 EURITRACK project, FP6-2003-IST-2 Proposal/Contract no. 511471. The authors specially thank Croatian Custom Office of Rijeka and Rijeka Seaport Authorities, Croatia, who allowed the implementation of the EURITRACK system in Rijeka and its continuing operation for the Eritr@C project. We are also very grateful to the EURITRACK partners who contributed to the development and commissioning of the system: INFN (Italy), JRC (Italy), CAEN (Italy), SODERN (France), and IPJ (Poland).

References

Bendahan, J., Clayton, J., Fankhauser, K., Gozani, T., Krivicich, J., Loveman, R., Pentaleri, E., Ryge, P., Sawa, P., Stevenson, J., 1995. Nucl. Instrum. Meth. B 99, 505.

Buffler, A., Tickner, J., 2010. Detecting contraband using neutrons: challenges and future directions. Radiat Meas 45, 1186–1192.

Carasco, C., Pérot, B., et al., 2007. Photon attenuation and neutron moderation correction factors for the inspection of cargo containers with tagged neutrons. Nucl. Instrum. Meth. A 582, 638–643.

Carasco, C., 2010. Comput. Phys. Commun. 181, 1161.

Carasco, C., Pérot, B., et al., 2008. In-field tests of the EURITRACK tagged neutron inspection system. Nucl. Instrum. Meth. A 588, 397–405.

Day, Robert B., Walt, Martin, 1960. Physical Review 117 (5).

EvseninA.V. , GorshkovI.Yu. , et al., Detection of explosives and other illicit materials by nanosecond neutron analysis In: Proceedings of the International Topical Meeting on Nuclear Research Applications and Utilization of Accelerators, 4–8 May 2009, Vienna.

El Kanawati, W., Perot, B., Carasco, C., Eléon, C., Valkovic, V., Sudac, D., Obhodas, J., Sannie, G., 2011a. Acquisition of prompt gamma-ray spectra induced by 14 MeV neutrons and comparison with Monte Carlo simulations. Appl. Radiat. Isot. 69, 732–743.

El Kanawati, W., Carasco, C., Pérot, B., et al., 2010. Gamma-Ray signatures improvement of the EURITRACK Tagged Neutron Inspection System Database. IEEE. Trans.. Nucl. Sci. 57 (5), 2879–2885 October.

El KanawatiW. , PerotB. , CarascoC. , EleonC. , ValkovicV. , SudacD. , ObhodasJ. , Conversion Factors from Counts to Chemical Ratios for the EURITRACK Tagged Neutron Inspection System, Nucl. Instrum. Meth. A, in press, org/10.1016/j.nima.2011b.05.076.

Lunardon, M., et al., 2007. Front-end electronics and DAQ for the EURITRACK tagged neutron inspection system. Nucl. Instrum. Meth. B 261, 391.

RSICCMonte Carlo N–particle transport code system including MCNP5 1.40 and MCNPX 2.5.0 and data libraries. RSICC code package CCC-0730.

Obhodas, J., Sudac, D., Valkovic, V., et al., 2010. Nucl. Instrum. Meth. A 619, 460–466.

Perot, B., Carasco, C., Bernard, S., Mariani, A., Szabo, J.-L., Sannie, G., Valkovic, V., Sudac, D., Viesti, G., Lunardon, M., et al., 2008. Appl. Radiat. Isot. 66, 421.

SimakovS.P. , PavlikA. , VonachH. , HlavacS. , 1998. Status of experimental and evaluated discrete gamma-ray production at En=14.5 MeV. IAEA Nuclear Data Section, INDC(CCP)-413, available from 〈http://www-nds.iaea.org/reports-new/indc-reports/indc-ccp/〉.

Valkovic, V., Miljanic, D., Tomas, P., Antolkovic, B., Furic, M., 1969. Nucl. Instrum. and Meth. 76, 29.